$InFeBr_3$ and $InMnBr_3$: Synthesis, Crystal Structure, Magnetic Properties, and Electronic Structure

Richard Dronskowski[†]

Max-Planck-Institut für Festkörperforschung, Heisenbergstrasse 1, 70 569 Stuttgart, Germany

Received May 4, 1994[⊗]

Yellow and pink crystals of $InFeBr_3$ and $InMnBr_3$, the first structurally characterized transition metal bromides containing univalent indium, are synthesized from elemental Fe/Mn and molten $InBr_3$. The orthorhombic crystal structures ($InFeBr_3$: $a = 934.81(9)$ pm, $b = 394.35(4)$ pm, $c = 1514.1(2)$ pm; $InMnBr_3$: $a = 943.1(1)$ pm, $b = 398.95(4)$ pm, $c = 1535.3(2)$ pm; *Pnma*, $Z = 4$) are isotypic with NH_4CdCl_3. While the transition metals cations are octahedrally coordinated by Br^- anions, monovalent indium cations are found in strongly distorted trigonal Br^- prisms which are tricapped by additional Br^- anions. $InFeBr_3$ and $InMnBr_3$ show Curie-Weiss paramagnetism whereas only $InFeBr_3$ exhibits antiferromagnetic ordering below 15 K. Semiempirical band structure calculations (CSC-EH-TB) reflect strongly covalent contributions to In^+-Br^- bonding, exceeding those interactions found in the binary In/Br crystal chemical system. Moreover, there is weak In^+-In^+ bonding between neighboring unit cells. Valence charge density plots based on *ab initio* band structure computations (TB-LMTO-ASA) disprove the existence of a directional electron "lone-pair" centered on monovalent In.

1. Introduction

Indium in its univalent oxidation state shows an astonishingly large number of particularly unfamiliar coordination polyhedra, a fact that is most easily demonstrated by looking at the crystal chemistry of the binary indium bromides.[1-5] A recent quantum mechanical bonding study on the latter class of materials revealed the cause of this phenomenon to lie in the presence of the filled indium 5s atomic orbital at the frontier bands.[6] Any coordination polyhedron giving sufficient space for In^+, aside from repulsive anion-anion interactions, is equally appropriate and leads to similar bonding energies.

In order to further investigate the crystal chemistry of monovalent indium by both synthetic and theoretical methods, we have performed a study concerning the reactivity of molten indium bromides with respect to other metallic elements. Here we report on the synthesis, crystal structure, magnetic properties, and electronic structures of $InFeBr_3$ and $InMnBr_3$, the first structurally characterized transition metal bromides containing univalent indium.

2. Experimental and Theoretical Techniques

2.1. Synthesis. $InFeBr_3$ and $InMnBr_3$ were synthesized in quantitative yields by heating equimolar amounts of freshly prepared $InBr_3$ and the corresponding metals in evacuated glass ampoules at 450 °C for 5 days. $InBr_3$ itself was made from aqueous solution[7] and purified by repeated sublimation. The metals (Merck, p.a.) were used as purchased. The melts were cooled down to 100 °C at a rate of 2 °C/h, then to room temperature at 20 °C/h.

$InFeBr_3$ and $InMnBr_3$ crystallize as yellow and pink transparent needles. $InFeBr_3$ crystals are macroscopically twinned along the needle axis but they can be broken into their single components with some effort. Both compounds are extremely sensitive to humidity and were handled in an argon filled glovebox and sealed into glass (quartz) capillaries for X-ray and thermoanalytical studies.

2.2. Crystal Structure Analysis. Powder investigations revealed the presence of an orthorhombic crystal system. An X-ray Guinier diagram of $InFeBr_3$ shows the following characteristic reflections (d value in pm (hkl) relative intensity): 444.1 (103) 16, 295.6 (211) 100, 294.9 (113) 46, 294.2 (204) 38, 288.2 (302) 22, 288.1 (105) 44, 280.0 (212) 57, 262.1 (114) 20, 240.6 (304) 12, 240.2 (015) 18, 205.4 (314) 28, 197.2 (020) 31, 186.8 (413) 12, 185.9 (117) 20, 167.9 (118) 12, 163.8 (224) 15, 162.7 (125) 18, 157.3 (416) 15, 148.0 (309) 13, 126.1 (231) 11, 118.4 (329) 17. For $InMnBr_3$ the characteristic reflections are as follows: 449.8 (103) 14, 298.8 (211) 100, 298.5 (113) 46, 297.7 (204) 36, 292.0 (105) 50, 290.9 (302) 21, 283.1 (212) 63, 265.4 (114) 20, 243.3 (015) 19, 243.2 (304) 12, 207.7 (314) 28, 199.5 (020) 31, 188.7 (413) 11, 188.3 (117) 21, 170.1 (118) 10, 165.7 (224) 14, 164.7 (125) 20, 159.0 (416) 15, 149.9 (309) 13, 127.6 (231) 10, 119.9 (329) 17. For obtaining greater precision, the lattice constants of $InFeBr_3$ and $InMnBr_3$ were refined on the basis of powder data (Stoe powder diffractometer).

Axes photographs of single crystals confirmed the crystal class. Complete sets of intensities at room temperature were obtained (Enraf-Nonius CAD4 four circle diffractometer, Mo-Kα radiation, graphite monochromator, scintillation counter) between 5–60° in 2θ ($-13 \le h \le 0$, $-5 \le k \le 5$, $-21 \le l \le 0$) by speed-varying, prescan-dependent $\omega-\theta$ scans. The data sets were reduced and corrected semi-empirically for absorption.[8] The systematic absences indicated space groups $Pna2_1$ or *Pnma* with only one weak ($I \approx 4\sigma(I)$) violation for an axis reflection (010) of the Mn compound.

The structure was solved in *Pnma* by use of direct methods (SHELXS-86),[9] giving all atomic positions. Subsequent least squares, full matrix isotropic and anisotropic refinements (SHELXL-93)[10] using scattering factors of the neutral atoms[11] converged successfully and confirmed the chemical formulas. After including extinction effects in the refinements, the R_1 residuals[12] were 0.043 ($InFeBr_3$) and 0.059 ($InMnBr_3$). Refinements in the acentric space group $Pna2_1$, on the other hand, led to wR_2 residuals that were larger by more than 0.02. More

† drons@simix.mpi-stuttgart.mpg.de.

⊗ Abstract published in *Advance ACS Abstracts,* November 1, 1994.

(1) Staffel, T.; Meyer, G. *Z. Anorg. Allg. Chem.* **1987**, *552*, 113.
(2) Staffel, T.; Meyer, G. *Z. Anorg. Allg. Chem.* **1988**, *563*, 27.
(3) Marsh, R. E.; Meyer, G. *Z. Anorg. Allg. Chem.* **1990**, *582*, 128.
(4) Bärnighausen, H. *Z. Kristallogr.* **1989**, *186*, 16.
(5) Beck, H. P. *Z. Naturforsch.* **1987**, *42b*, 251.
(6) Dronskowski, R. *Inorg. Chem.*, in press. The value for the optimum single bond distance r_0 is based on 107 In^+-Br^- bond lengths, all of them from the crystal structures of the binary indium bromides.
(7) Ensslin, F.; Dreyer, H. *Z. Anorg. Allg. Chem.* **1942**, *249*, 119.
(8) North, A. C. T.; Phillips, D. C.; Mathews, F. S. *Acta Crystallogr.* **1968**, *A24*, 351.
(9) Sheldrick, G. M. *Acta Crystallogr.* **1990**, *A46*, 467.
(10) Sheldrick, G. M. *J. Appl. Crystallogr.*, in preparation.
(11) *International Tables for Crystallography, Volume C*; Wilson, A. J. C., Ed.; Kluwer Academic Publishers: Dordrecht, 1992.

0020-1669/94/1333-5927$04.50/0

Table 1. Crystallographic Data for $InFeBr_3$

chem formula: $InFeBr_3$	fw = 410.38
a = 934.81(9) pm	space group: *Pnma* (No. 62)
b = 394.35(4) pm	λ = 71.073 pm
c = 1514.1(2) pm	ϱ_{calcd} = 4.884 g/cm^3
$V = 558.1(1) \times 10^6$ pm^3	μ = 28.03 mm^{-1}
Z = 4	R_1 ($F_o > 4\sigma(F_o)$)[12] = 0.043
T = 20(1) °C	wR_2 (all data)[12] = 0.085

Table 2. Crystallographic Data for $InMnBr_3$

chem formula: $InMnBr_3$	fw = 409.47
a = 943.1(1) pm	space group: *Pnma* (No. 62)
b = 398.95(4) pm	λ = 71.073 pm
c = 1535.3(2) pm	ϱ_{calcd} = 4.709 g/cm^3
$V = 577.6(1) \times 10^6$ pm^3	μ = 26.76 mm^{-1}
Z = 4	R_1 ($F_o > 4\sigma(F_o)$)[12] = 0.059
T = 20(1) °C	wR_2 (all data)[12] = 0.144

Table 3. Positional Parameters (All Atoms on Special Position 4*c*, $y \equiv 1/4$) and Isotropic Displacement Parameters[a] (pm^2) for $InFeBr_3$ (Standard Deviations in Parentheses)

atom	x	z	U_{eq}
In	0.4494(1)	0.67335(7)	507(3)
Fe	0.1597(2)	0.4454(1)	293(4)
Br(1)	0.6763(1)	0.49765(8)	297(3)
Br(2)	0.2725(1)	0.29288(7)	339(3)
Br(3)	0.0249(1)	0.60045(7)	276(3)

[a] U_{eq} is a third of the trace of the orthogonalized U_{ij} tensor.

Table 4: Positional Parameters (All Atoms on Special Position 4*c*, $y \equiv 1/4$) and Isotropic Displacement Parameters[a] (pm^2) for $InMnBr_3$ (Standard Deviations in Parentheses)

atom	x	z	U_{eq}
In	0.4471(2)	0.67645(8)	491(4)
Mn	0.1626(2)	0.4441(1)	275(5)
Br(1)	0.6723(1)	0.49708(9)	276(3)
Br(2)	0.2786(2)	0.28980(9)	328(4)
Br(3)	0.0245(1)	0.60194(8)	252(3)

[a] U_{eq} is a third of the trace of the orthogonalized U_{ij} tensor.

important, the standard deviations for the positional parameters increased by more than one order of magnitude, suggesting that $InFeBr_3$ and $InMnBr_3$ are indeed centrosymmetric.

For all atoms, the components of the anisotropic displacement factors are very well behaved. It is interesting to note that the isotropic displacement factor of In is more than 30 per cent larger than those of the other atoms although the indium position is fully occupied (1.000(4) in the Fe, 0.993(5) in the Mn compound). This is typical for univalent indium, finding its explanation in the local electronic structure:[13] In^+ is residing in a very soft crystal potential, allowing "trembling motions" around the equilibrium position.

The final difference Fourier maps were flat, the strongest residual peaks were about 87 (103) pm away from the Br(3) atom of $InFeBr_3$ ($InMnBr_3$). Tables 1 and 2 show all relevant data of the structure analysis while Tables 3 and 4 contain positional and isotropic displacement parameters. Selected interatomic distances are given in Tables 5 and 6.[14]

2.3. Magnetic Measurements. Crystalline samples of 68 mg $InFeBr_3$ and 170 mg $InMnBr_3$ were subjected to susceptibility measurements by use of a Quantum Design MPMS 5.5 Squid susceptometer within a temperature range of 2−300 K at a field strength of 1 kG. The influence of the electron core shells on the molar susceptibilities was corrected using tabulated diamagnetic values for the different ions.[15] The value for In^+ (-23×10^{-6} emu/mol) was taken from a previous investigation.[16]

Table 5. Selected Interatomic Distances (pm) in $InFeBr_3$ (Standard Deviations in Parentheses)[a]

In−Br(2d)	330.2(1)	In−In(b)	394.35(4)
−Br(2c)	330.2(1)	−In(a)	394.35(4)
−Br(2i)	338.6(1)	−Fe	438.7(2)
−Br(2j)	338.6(1)		
−Br(1)	340.2(2)		
−Br(1c)	346.0(1)		
−Br(1d)	346.0(1)		
−Br(3l)	349.7(2)		
−Br(3)	411.9(2)		
Fe−Br(2)	253.9(2)	Fe−Fe(g)	394.2(3)
−Br(1d)	264.2(1)	−Fe(h)	394.2(3)
−Br(1c)	264.2(1)	−Fe(a)	394.35(4)
−Br(3)	266.4(2)	−Fe(b)	394.35(4)
−Br(3g)	271.1(1)		
−Br(3h)	271.1(1)		
Br(1)−Br(3k)	361.2(2)	Br(2)−Br(3g)	377.2(1)
−Br(3d)	372.7(1)	−Br(3h)	377.2(1)
−Br(3c)	372.7(1)	−Br(2a)	394.35(4)
−Br(2d)	376.5(1)	−Br(2b)	394.35(4)
−Br(2c)	376.5(1)	−Br(3e)	399.5(1)
−Br(1c)	384.2(2)	−Br(3f)	399.5(1)
−Br(1d)	384.2(2)		
−Br(1b)	394.35(4)		
−Br(1a)	394.35(4)		
Br(3)−Br(3g)	365.5(2)		
−Br(3h)	365.5(2)		
−Br(3b)	394.35(4)		
−Br(3a)	394.35(4)		

[a] Symmetry coding (including lattice translations): (a) x, $y-1$, z; (b) x, $y+1$, z; (c) $-x+1$, $-y$, $-z+1$; (d) $-x+1$, $-y+1$, $-z+1$; (e) $-x+1/2$, $-y$, $z-1/2$; (f) $-x+1/2$, $-y+1$, $z-1/2$; (g) $-x$, $-y$, $-z+1$; (h) $-x$, $-y+1$, $-z+1$; (i) $-x+1/2$, $-y$, $z+1/2$; (j) $-x+1/2$, $-y+1$, $z+1/2$; (k) $x+1$, y, z; (l) $x+1/2$, y, $-z+3/2$.

2.4. Thermoanalytical Investigations. Differential thermoanalytical analyses on $InFeBr_3$ and $InMnBr_3$ were performed with the help of a Heraeus DTA 500 instrument. The samples of about 500 mg were sealed into evacuated thin walled quartz capillaries and a temperature range of 30−400 °C was scanned with a scan speed of 5 °C per minute.

Another sample of crystalline $InFeBr_3$ was investigated by the temperature-varying Guinier-Simon powder X-ray technique.[17] The temperature range was 26−387 °C and the scan speed 7.7 °C per hour.

2.5. Electronic Structure Investigations. Electronic structure calculations on $InFeBr_3$ and $InMnBr_3$ followed two different routes. Semi-empirical tight-binding calculations were used for analyzing the chemical bonding whereas first principles computations had to be performed for the generation of charge density plots. Neither a numerical comparison of the two approaches nor a fit of the semi-empirical parameters to the *ab initio* results was attempted. Thus, the standard semi-empirical calculational technique performed here could be directly compared with a recent study on the electronic structure of the binary indium bromides.[6] Second, since both compounds are Curie-Weiss paramagnets (see Section 3.4), the first principles calculations were done in spin-polarized mode, an approach which is practically impossible to perform with a semi-empirical procedure. All computations were carried out either on a DECstation 5000/133 or on an IBM RS 6000/520 machine, running under the UNIX operating system.

(12) R_1 is only for comparison with conventional structure factor F refinements. Note that SHELXL-93 refines against F^2 in order to minimize the so-called wR_2 residual. The latter is indeed based on F^2 and statistically about twice as large as those based on F. The definitions are as follows:

$$wR_2 = \sqrt{\Sigma[w(F_o^2 - F_c^2)^2]/\Sigma[w(F_o^2)^2]}$$

$$R_1 = \Sigma||F_o| - |F_c||/\Sigma(F_o)$$

(13) Dronskowski, R.; Schönberger, U., Manuscript on energy hypersurfaces of In^+ inside Br^- polyhedra in preparation.

(14) A list of the observed and calculated structure factors may be obtained from the Fachinformationszentrum Karlsruhe, D-76344 Eggenstein-Leopoldshafen, on quoting the depository number CSD-58486, the author's name, and the journal citation.

(15) Selwood, P. W.; *Magnetochemistry*, 2nd ed.; Interscience Publishers: New York, 1956.
(16) Dronskowski, R. Ph.D. Thesis, Universität Stuttgart (FRG), 1990.
(17) Simon, A. *J. Appl. Crystallogr.* **1970**, *3*, 17.

Table 6. Selected Interatomic Distances (pm) in $InMnBr_3$ (Standard Deviations in Parentheses)[a]

In−Br(2d)	330.8(2)	In−In(b)	398.95(4)
−Br(2c)	330.8(2)	−In(a)	398.95(4)
−Br(2i)	339.6(2)	−Mn	446.4(2)
−Br(2j)	339.6(2)		
−Br(1)	347.8(2)		
−Br(3l)	348.0(2)		
−Br(1c)	351.3(2)		
−Br(1d)	351.3(2)		
−Br(3)	414.7(2)		
Mn−Br(2)	260.9(2)	Mn−Mn(b)	398.95(4)
−Br(1d)	268.7(2)	−Mn(a)	398.95(4)
−Br(1c)	268.7(2)	−Mn(g)	404.2(3)
−Br(3)	275.2(2)	−Mn(h)	404.2(3)
−Br(3g)	275.5(2)		
−Br(3h)	275.5(2)		
Br(1)−Br(3k)	369.1(2)	Br(2)−Br(3g)	386.1(2)
−Br(3d)	380.4(2)	−Br(3h)	386.1(2)
−Br(3c)	380.4(2)	−Br(3e)	396.8(2)
−Br(1c)	381.4(2)	−Br(3f)	396.8(2)
−Br(1d)	381.4(2)	−Br(2b)	398.95(4)
−Br(2d)	386.0(2)	−Br(2a)	398.95(4)
−Br(2c)	386.0(2)		
−Br(1b)	398.95(4)		
−Br(1a)	398.95(4)		
Br(3)−Br(3g)	374.0(2)		
−Br(3h)	374.0(2)		
−Br(3a)	398.95(4)		
−Br(3b)	398.95(4)		

[a] Symmetry coding (including lattice translations): (a) $x, y-1, z$; (b): $x, y+1, z$; (c) $-x+1, -y, -z+1$; (d) $-x+1, -y+1, -z+1$; (e) $-x+{}^1/_2, -y, z-{}^1/_2$; (f) $-x+{}^1/_2, -y+1, z-{}^1/_2$; (g) $-x, -y, -z+1$; (h) $-x, -y+1, -z+1$; (i) $-x+{}^1/_2, -y, z+{}^1/_2$; (j): $-x+{}^1/_2, -y+1, z+{}^1/_2$; (k) $x+1, y, z$; (l) $x+{}^1/_2, y, -z+{}^3/_2$.

2.5.1. Semiempirical Calculations. The semi-empirical calculations on $InFeBr_3$ and $InMnBr_3$ were started from tabulated Coulomb integrals using a simplified one-electron Hamiltonian as in charge-self-consistent[18] extended Hückel theory.[19] Within the iterative process towards self-consistency, the amount of electron correlation was corrected up to first order by varying all atomic Coulomb integrals dependent on atomic charge and electronic configuration. To do so, the charge dependence of the valence orbitals' ionization potentials was approximated through a quadratic power series. The explicit charge iteration parameters for In and Br were the same as in a related study[6] whereas those of Fe and Mn were taken from the original literature.[18]

Slater-type orbital exponents for In and Br were based on numerical atomic wave-functions given in Pyykkö and Lohr's compilation[20] whereas those of Fe and Mn were taken from the work of Fitzpatrick and Murphy (Herman-Skillman fits).[21] A minimal set of Slater functions for In (5s,5p), Br (4s,4p), Fe (4s,4p,3d), and Mn (4s,4p,3d) was used throughout. The amount of counterintuitive orbital mixing within the minimal basis set was minimized by computing the off-site Hamiltonian matrix elements as defined in the weighted WH-formula.[22] The eigenvalue problem was solved in reciprocal space at 42 k points within the irreducible wedge of the Brillouin zone using a modified EHMACC code.[23] The resulting exchange integrals and the basis sets used are tabulated in Tables 7 and 8.

2.5.2. First-Principles Calculations. Electronic structure calculations of *ab initio* quality were performed using LMTO (Linear Muffin-Tin Orbital) theory,[24-27] a linearized form of the KKR method.[28,29] The method accounts for the potential from all the electrons and is applicable to materials composed of atoms from any part of the periodic table. Their almost minimal, unfixed basis sets adjust dynamically to the respective potentials. In the interstitial regions with flat potentials, the wave functions of the valence electrons are expanded into Hankel envelope functions whereas in the core-like regions one seeks numerical solutions of the radial Schrödinger equation.

Table 7. Slater Orbital Exponents and Charge-Iterated Exchange Integrals for $InFeBr_3$

atom	orbital	ζ	H_{ii} (eV)
In	5s	1.934	−11.983
	5p	1.456	−6.986
Fe	4s	1.430	−6.650
	4p	0.972	−3.353
	3d[a]		−8.675
Br(1)	4s	2.588	−23.291
	4p	2.131	−11.076
Br(2)	4s	2.588	−23.492
	4p	2.131	−11.423
Br(3)	4s	2.588	−22.935
	4p	2.131	−10.464

[a] Fe d orbitals were approximated by double-ζ functions with exponents $\zeta_1 = 5.653$ and $\zeta_2 = 2.325$ and weighting coefficients $c_1 = 0.485$ and $c_2 = 0.661$.

Table 8. Slater Orbital Exponents and Charge-Iterated Exchange Integrals for $InMnBr_3$

atom	orbital	ζ	H_{ii} (eV)
In	5s	1.934	−11.870
	5p	1.456	−6.892
Mn	4s	1.374	−6.725
	4p	0.949	−3.511
	3d[a]		−8.345
Br(1)	4s	2.588	−23.166
	4p	2.131	−10.861
Br(2)	4s	2.588	−23.452
	4p	2.131	−11.355
Br(3)	4s	2.588	−22.933
	4p	2.131	−10.460

[a] Mn d orbitals were approximated by double-ζ functions with exponents $\zeta_1 = 5.318$ and $\zeta_2 = 2.176$ and weighting coefficients $c_1 = 0.481$ and $c_2 = 0.666$.

For $InFeBr_3$ and $InMnBr_3$, the electronic energy was computed with the help of density-functional theory, replacing the many-particle problem by the self-consistent solution of the Kohn-Sham equations,[30,31] parametrized according to von Barth and Hedin.[32] The Hamiltonian allowed for a spin-polarized scalar relativistic calculation of the electronic structure. The integration in k space was done with the help of an improved[33] tetrahedron method[34] using 16 inequivalent k points and 123 different tetrahedra. A minimal basis set of short-range atom-centered TB-LMTO's was used throughout the investigation,[35] this is with one s, three p, and five d orbitals on each of the atoms. Indium and bromine d orbitals were included using a downfolding technique. Starting from atomic Hartree potentials, the structure was iterated by

(18) McGlynn, S. P.; Vanquickenborne, L. G.; Kinoshita, M.; Carroll, D. G. *Introduction to Applied Quantum Chemistry*; Holt, Rinehart and Winston: New York, 1972.
(19) Hoffmann, R. *J. Chem. Phys.* **1963**, *39*, 1397.
(20) Pyykkö, P.; Lohr, L. L., Jr. *Inorg. Chem.* **1981**, *20*, 1950.
(21) Fitzpatrick, N. J.; Murphy, G. H. *Inorg. Chim. Acta* **1984**, *87*, 41; **1986**, *111*, 139.
(22) Ammeter, J. H.; Bürgi, H.-B.; Thibeault, J. C.; Hoffmann, R. *J. Am. Chem. Soc.* **1978**, *100*, 3686.
(23) QCPE program EHMACC. Whangbo, M.-H.; Evain, M.; Hughbanks, T.; Kertesz, M.; Wijeyesekera, S.; Wilker, C.; Zheng, C.; Hoffmann, R.
(24) Andersen, O. K. *Phys. Rev. B* **1975**, *12*, 3060.
(25) Andersen, O. K.; Jepsen, O.; Glötzel, D. In *Highlights of Condensed-Matter Theory*; Bassani, F. *et al.*, Eds.; North-Holland: New York, 1985.
(26) Skriver, H. L. *The LMTO Method*; Springer: Berlin, Heidelberg, New York, 1984.
(27) Andersen, O. K.; Jepsen, O.; Sob, M. In *Electronic Band Structure and its Applications*; Yussouff, M., Ed.; Springer: Berlin, Heidelberg, New York, 1986.
(28) Korringa, J. *Physica* **1947**, *13*, 392.
(29) Kohn, W.; Rostoker, N. *Phys. Rev.* **1954**, *94*, 1111.
(30) Hohenberg, P.; Kohn, W. *Phys. Rev.* **1964**, *136*, B 864.
(31) Kohn, W.; Sham, L. J. *Phys. Rev.* **1965**, *140*, A 1133.
(32) von Barth, U.; Hedin, L. *J. Phys. C* **1972**, *5*, 1629.
(33) Blöchl, P. Ph.D. Thesis, Universität Stuttgart (FRG), 1989.
(34) Jepsen, O.; Andersen, O. K. *Solid State Commun.* **1971**, *9*, 1763.
(35) Andersen, O. K.; Jepsen, O. *Phys. Rev. Lett.* **1984**, *53*, 2571.

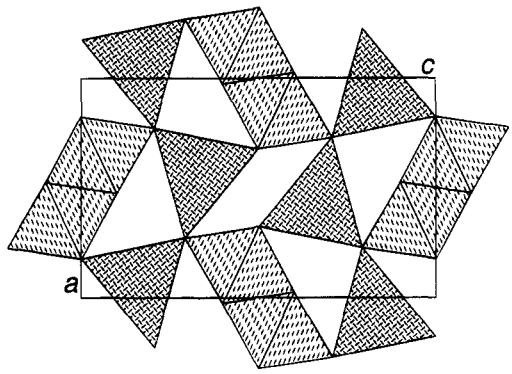

Figure 1. Polyhedral projection of the $InFeBr_3$ ($InMnBr_3$) crystal structure along the *b* axis. The In^+ ions are located inside trigonal Br^- prisms (herringbone pattern) whereas the transition metal cations are found in vertice-sharing Br^- octahedra (dashed lines). See text for more details.

use of the atomic-spheres approximation (ASA), employing muffin-tin spheres blown up to overlapping and volume filling spheres. A combined correction term was included. After having reached self-consistency, charge density plots were generated upon switching to full-potential LMTO mode, dropping any shape approximations for the potential inside the crystal. The program used was TB-LMTO 4.4.[36]

3. Results and Discussion

3.1. Description of the Crystal Structure. $InFeBr_3$ and $InMnBr_3$ crystallize in the NH_4CdCl_3 structure type, a projection of which is given in Figure 1. Iron and manganese ions of oxidation state +II are coordinated by six bromine anions to form slightly distorted octahedra. The average $Fe^{2+}-Br^-$ ($Mn^{2+}-Br^-$) bond length is 265.2 (270.8) pm and individual bond length deviations from this value are smaller than 11 ($InFeBr_3$) and 10 pm ($InMnBr_3$). Any such octahedron is laterally connected with four other octahedra by sharing five of its vertices such that there results a double chain of octahedra running along the short *b* axis.

The univalent indium cations, on the other hand, are located in significantly distorted trigonal prisms, one of the two depicted in Figure 2. The prism's three rectangular faces are capped by other bromine ions whereas the top and the bottom face is covered by the neighbor unit cells' indium ions, giving rise to indium-indium contacts of 398.95 ($InFeBr_3$) and 394.35 pm ($InMnBr_3$) that allow some weak interaction.

The above grouping of the coordinating bromine ions is admittedly idealized. First, the three main In^+-Br^- bond lengths inside the prism (each occuring twice) cover a range of 330−346 pm ($InFeBr_3$) and of 331−351 pm ($InMnBr_3$). Second, at least one of the "outer" face-capping Br^- ions (Br-(1) in Figure 2) has a quite short In^+-Br^- bond length, namely 340 ($InFeBr_3$) and 348 pm ($InMnBr_3$), even shorter than the longest intra-prism In^+-Br^- bond distance. Third, there is a large variance in the In^+-Br^- bond lengths of the face-capping Br^- ions themselves. Here one finds distances of 340, 350, and 412 pm for $InFeBr_3$ and of 2 × 348 and 415 pm for $InMnBr_3$. In other words, there is one face-capping ligand (Br-(3) in Figure 2) which is about 20 per cent further away from the indium cation. Within classic crystal chemistry, heavily influenced by electrostatic reasoning, it has become popular to interpret such geometrical distortions by assuming a stereoactive electron "long-pair" residing on the indium ion. For example, a well-known monograph on crystal chemistry[37] proposes hypothetical main group metal ion-lone pair distances (86 pm for In^+).[38] We will touch on this theoretical concept in the electronic structure part of this paper.

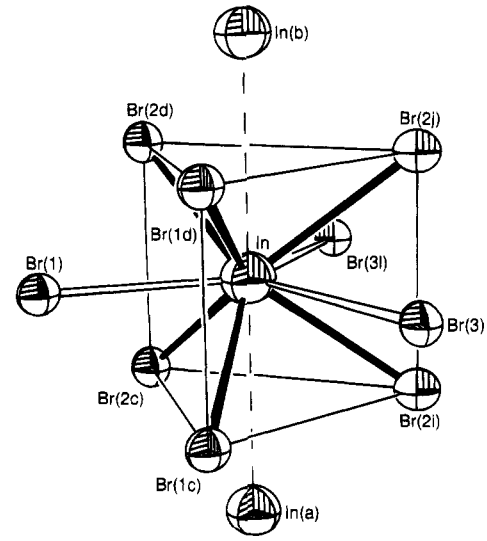

Figure 2. Perspective view of the In^+ coordination by Br^- ions in $InFeBr_3$ (and similarly in $InMnBr_3$). The ellipsoids enclose 70% of the electrons' spatial probability. In^+-Br^- bonds are given as solid (Br^- ions inside trigonal prism) and open lines (face capping Br^- ions) whereas the shortest In^+-In^+ contacts are drawn with broken lines. The edges of the trigonal prism are emphasized by thin lines.

3.2. Ionic Radii and Volume Considerations. Not long ago, Tournoux and coworkers[39] synthesized the isotypic compound β-$TlFeBr_3$, a low-temperature variant of hexagonal $TlFeBr_3$ which is stable above 384 °C.[40] As is obvious from the positional and lattice parameters, green β-$TlFeBr_3$ is intimately related to the here characterized yellow $InFeBr_3$. For example, the average $Fe^{2+}-Br^-$ distance in β-$TlFeBr_3$ is 265.6 pm, equivalent within two standard deviations (0.2 pm) to the value of $InFeBr_3$. However, there is one puzzling phenomenon:

Judging from ionic radii,[41] In^+ is about 17 pm smaller than Tl^+. Consequently, one would expect an increase in molar volume of about 2.54 cm^3/mol upon going from $InFeBr_3$ to β-$TlFeBr_3$, provided that those ionic radii are approximately additive. A similar conclusion can even more directly be drawn from Biltz's classic compilation[42] of atomic (ionic) volume increments. Here the increase should be 2.5 cm^3/mol in going from the indium to the thallium compound.

Whereas the *b* axis of β-$TlFeBr_3$ is indeed 1% larger than that of $InFeBr_3$, the *a* and *c* axes of the Tl compound are 0.7 and 0.5% *smaller* than those of the In phase. In total, the molar volume of β-$TlFeBr_3$ is *smaller* by 0.15 cm^3/mol than the molar volume of $InFeBr_3$, in sharp contrast to above ionic radii and volume considerations. Reconsidering the approximate equivalence of the $Fe^{2+}-Br^-$ distances between both phases, the difference in volume must arise from a difference in the In^+-(Tl^+)$-Br^-$ bond lengths. Indeed, the average In^+-Br^- distance is about 0.6 pm *longer* than the average Tl^+-Br^- distance of

(36) Program TB-LMTO 4.4 by van Schilfgaarde, M.; Paxton, T. A.; Jepsen, O.; Andersen, O. K.

(37) Hyde, B. G.; Andersson, S. *Inorganic Crystal Structures*; John Wiley & Sons: New York, Chichester, Brisbane, Toronto, Singapore, 1972.

(38) On the other hand (noted by a perceptive reviewer), the Valence Shell Electron Pair Repulsion (VSEPR) model predicts that the non-bonding electron pair will be closer to the atomic nucleus than the bonding electrons, *i.e.* the valence shell electrons will be polarized *away* from the non-bonding direction.

(39) Jouini, N.; Guen, L.; Tournoux, M. *Mater. Res. Bull* **1983**, *18*, 491.

(40) Jouini, N.; Guen, L.; Tournoux, M. *Mater. Res. Bull* **1982**, *17*, 1421.

(41) Emsley, J. *The Elements*, 2nd ed.; Clarendon Press: Oxford, England, 1991.

(42) Biltz, W. *Raumchemie der festen Stoffe*; Verlag von Leopold Voss: Leipzig, Germany, 1934.

347.3 pm, thus slightly widened and not moderately shortened as ionic radii/ionic volume arguments would lead us to expect.

One may assume the reason of this finding to lie in the In^+-Br^- bond lengths being too large, thereby giving the In^+ ion a too low bond valence sum. However, the calculation of such an empirical valence according to the empirical one-parameter formula of Brown and Altermatt,[43] using the recently evaluated optimum single bond distance r_0 of 266.7 pm,[6] gives a formal charge of +1.14. In other words, the empirical valence of indium is surely at the upper limit and the In^+-Br^- bond lengths appear to be quite *short*. This is in perfect agreement with the results of semi-empirical electronic structure calculations (see Section 3.5).

The apparent phenomenon may be largely due to an unexpected small size for the univalent thallium cation. This effect is most probably related to a relativistic contraction, well-known in having strong impacts on the actual size of the heavy elements. As has been pointed out so clearly by Pyykkö and Desclaux,[44] this relativistic s contraction is of major importance for the difference between the fifth and the sixth row of the periodic table, most easily visualized from the sizes of Slater exponents that had been fitted to non-relativistic and relativistic numerical atomic wavefunctions: For example, there is a 4% increase in the 5s exponent for the In atom upon switching to a relativistic Hamiltonian, representing a slightly smaller atom. The corresponding increase in the Slater exponent for thallium, however, is more than 15%, indicating a much stronger contraction.[20,45]

Obviously (and still hard to understand), this quantum mechanical effect which manifests from the structural comparison between the isotypic indium and thallium compounds, is neither reflected in ionic radii compilations nor in volume chemistry tables. Both of the latter may need to be adjusted. However, in order not to overstate the small size difference between In^+ and Tl^+ found here, at the present time it is probably best to state that the sizes of In^+ and Tl^+ are *comparable*.

3.3. Phase Transitions. DTA investigations on $InMnBr_3$ between 30−400 °C do not show any thermal effects except the compound's melting point at 379 °C. For $InFeBr_3$, on the other hand, the melting point lies beyond 400 °C and there is a reversible phase transition apparent around 181 °C, also visible in the temperature-dependent X-ray powder diffraction diagram. The unknown diffraction pattern of the new phase, not resembling the one of high-temperature hexagonal $TlFeBr_3$, could not be satisfactorily indexed. These studies are continuing.

3.4. Magnetic Properties. Plots of molar susceptibilities and reciprocal molar susceptibilities as a function of the temperature are given in Figure 3 for $InFeBr_3$ and in Figure 4 for $InMnBr_3$. It is evident that both phases exhibit Curie-Weiss paramagnetism.

For $InMnBr_3$, a linear fit of the data between 15 and 300 K results in a Curie temperature Θ of −2.7 K and an effective moment μ_{eff} of 5.86 μ_B, in very good agreement with the spin-only value for an $S = {}^5/_2$ Mn^{2+} ion (5.92 μ_B).

For $InFeBr_3$, a similar fit of the data above 100 K leads to Θ = 28.0 K and μ_{eff} = 3.83 μ_B, the latter significantly smaller than the spin-only value for an $S = {}^4/_2$ Fe^{2+} ion (4.90 μ_B). This finding has been observed in two different samples, both of them showing such lowering of the effective moment that may be due to a magnetic anisotropy of the $InFeBr_3$ crystals (very fine needles). In the measurements, the direction of the magnetic field coincided with the crystallographic *b* axis, the axis paralleling the double chains of Fe centered octahedra (see Figure 1). Additionally, we note that there are clear deviations from the Curie-Weiss law over the entire temperature range which lead to a bent temperature-reciprocal molar susceptibility curve.

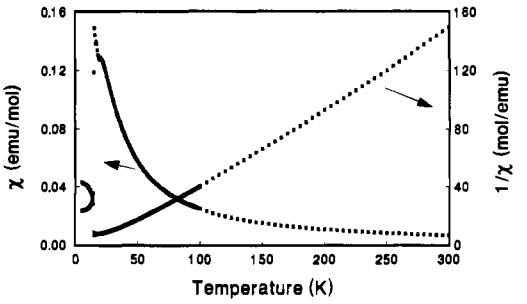

Figure 3. Molar susceptibility and reciprocal molar susceptibility as a function of the temperature for $InFeBr_3$ (H = 1 kG).

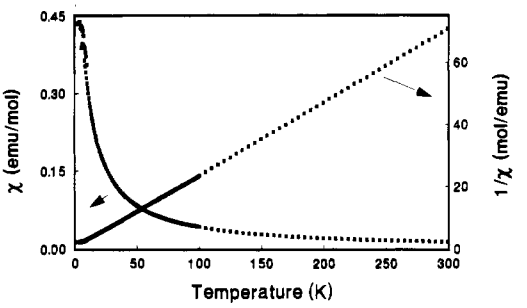

Figure 4. Same as in Figure 3 but for $InMnBr_3$.

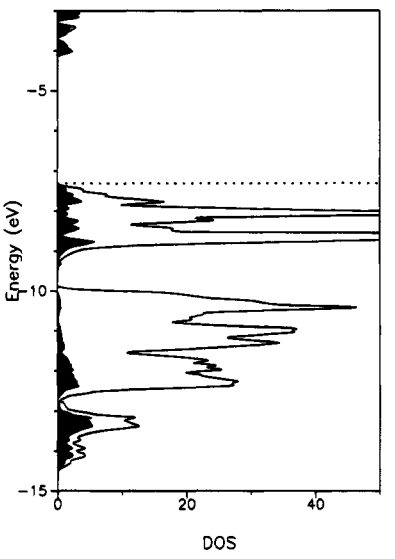

Figure 5. Density-of-states (DOS) of $InFeBr_3$ with In contributions emphasized in black.

For β-$TlFeBr_3$, showing more typical Curie-Weiss behavior, the published values are Θ = 12 K and μ_{eff} = 5.59 μ_B.[39] The effective moment seems to be rather large but no further information with respect to the shape of the samples or the direction of the magnetic field have been reported. In addition, $InFeBr_3$ is subject to antiferromagnetic ordering below a Néel temperature Θ_N of 15 K, very similar to β-$TlFeBr_3$ which has Θ_N = 14 K.

3.5. Electronic Structure. Figures 5 and 6 show the total and local (In) densities-of-states of $InFeBr_3$ and $InMnBr_3$, calculated using the semi-empirical method. In both cases, the In contributions can be decomposed into two main parts.

(43) Brown, I. D.; Altermatt, D. *Acta Crystallogr. B* **1985**, *41*, 244.
(44) Pyykkö, P.; Desclaux, J.-P. *Acc. Chem. Res.* **1979**, *12*, 276.
(45) Desclaux, J. P. *At. Data Nucl. Tables* **1973**, *12*, 311.

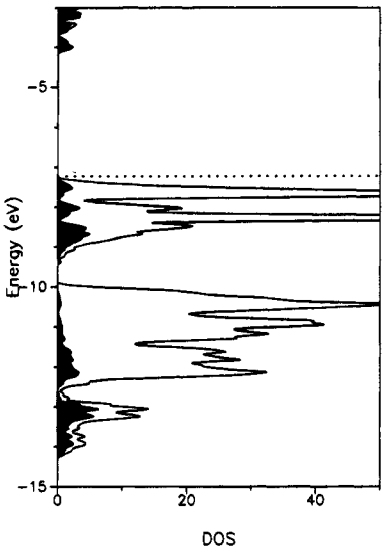

Figure 6. Same as in Figure 5 but for $InMnBr_3$.

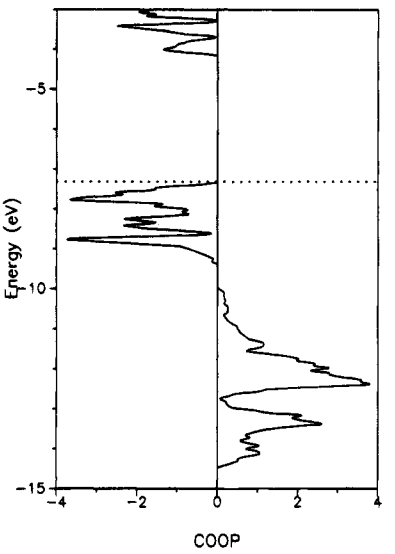

Figure 7. Crystal orbital overlap population (COOP) of the In^+-Br^- bonding (nine nearest bonds) in $InFeBr_3$.

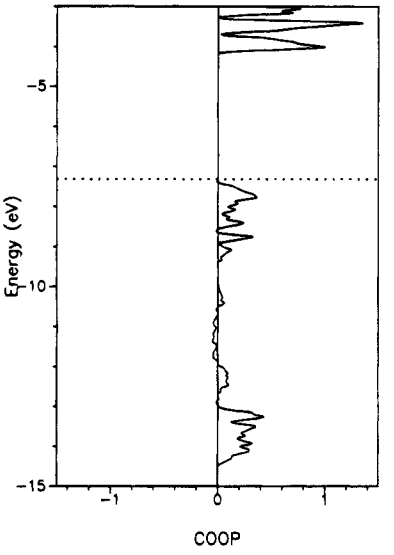

Figure 8. Crystal orbital overlap population (COOP) of the In^+-In^+ bonding (two contacts) in $InFeBr_3$.

Indium 5s atomic orbitals mix into the levels that lie either below about −13 eV or above −9.5 eV, going up to the Fermi level (dashed line). The contributions of the indium 5p orbitals, however, are significantly smaller, mixing in a little between −10 and approximately −12.7 eV, the region that is dominated by the Br 4p orbitals. Also, the virtual levels starting above −4 eV are practically 100% in indium 5p. Not shown are the strongly Br centered 4s bands below −23 eV.

The influence of the transition metals is easily appreciable from the bands just below the Fermi level. There is a 3d splitting visible which corresponds to the "e_g" and "t_{2g}" levels, resulting from the approximate octahedral Br^- environment of Fe^{2+} and Mn^{2+}. Note that some of these bands are only half-filled as has been shown from the magnetic measurements, and the bonding analysis that follows has been performed on the basis of the magnetic band filling as a consequence.

Concerning In^+-Br^- bonding with respect to the nine nearest Br^- neighbors around In^+, the crystal orbital overlap population[46] (COOP) plot in Figure 7 for $InFeBr_3$ (similar $InMnBr_3$ plot omitted for brevity) reflects a bonding pattern that is already known from the structures of, for example, InBr and $InBr_2$, both containing In^+ ions. In addition to the In^+-Br^- bonding levels below about −10 eV, there is a strongly *antibonding* region lying above that energy threshold, resulting from the out-of-phase combination between indium 5s and bromine 4p orbitals. This is common to all known In^+-Br^- interactions within crystalline solids.[6] More quantitatively, the values of the integrated crystal orbital overlap populations (ICOOP) are 0.169 ($InFeBr_3$) and 0.133 ($InMnBr_3$) which is surprisingly high for both cases. Note that In^+-Br^- ICOOP's in any of the binary indium bromides do not exceed a value of 0.084. In the present ternary compounds univalent indium ions are more firmly bound, an observation that also could have been guessed from the high bond valence sum of In^+ in $InFeBr_3$ (see discussion in Section 3.2). This strengthening of bonding inside a ternary phase would have been called a "salt effect" in classic coordination chemistry.

When it comes to transition metal−Br bonding, for future comparison reasons we give the ICOOP values which are 0.328 for $InFeBr_3$ and 0.344 for $InMnBr_3$. At this point, these values cannot be directly compared with each other since they depend on the (different) spatial extents of the wave functions centered on Fe and Mn atoms.

Next, we will focus on possible covalent bonding between indium ions of neighboring unit cells. In Figure 2, such a situation has been symbolized with broken lines. The corresponding COOP diagram is given in Figure 8 for $InFeBr_3$ ($InMnBr_3$ omitted). It is obvious that there are indeed some small bonding interactions, solely arising from the diffuse indium 5s atomic orbitals which have the largest spatial extent. Integrated up to the Fermi level, the ICOOP values are 0.088 ($InFeBr_3$) and 0.099 ($InMnBr_3$), running counterintuitive to the In^+-In^+ distance (length of the *b* axis) simply because of different electron fillings. One could have expected to find stronger In^+-In^+ interactions in the Mn phase (shorter *b* axis) than in the Fe compound. The ICOOP values are smaller than one third of the In^+-In^+ ICOOP in InBr where In−In bonding (355 pm distance) has been shown to play a significant role in structure stabilization.[6]

Finally, we come to the *ab initio* calculations. To start with, the iterations using a spin-polarized Hamiltonian converged to four unpaired electrons for $InFeBr_3$ and to five unpaired

(46) Crystal orbital overlap populations (COOP's) serve as quantitative and energy-resolved measures of bond strengths in solid state materials. The quantum mechanical analysis is typically based on three-dimensional band structure calculations using short-range basis sets. The COOP technique was invented by Hughbanks and Hoffmann: Hughbanks, T.; Hoffmann, R. *J. Am. Chem. Soc.* **1983**, *105*, 3528.

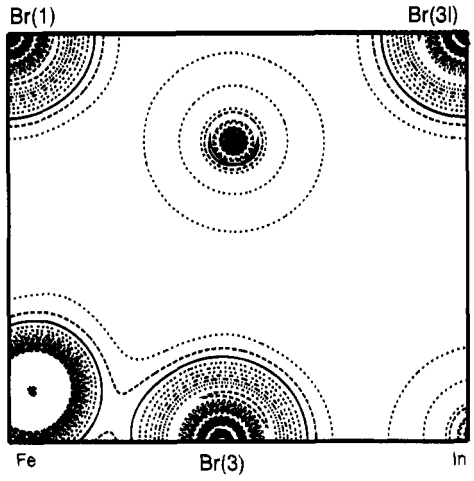

Figure 9. Computed charge density inside $InFeBr_3$ from first principles. The observable is given in 20 equidistant steps between 0 and 0.35 e/a_0^3 (a_0 is the Bohr radius which is about 53 pm). The outermost "ring" around the In atom (center) is 0.0175 e/a_0^3.

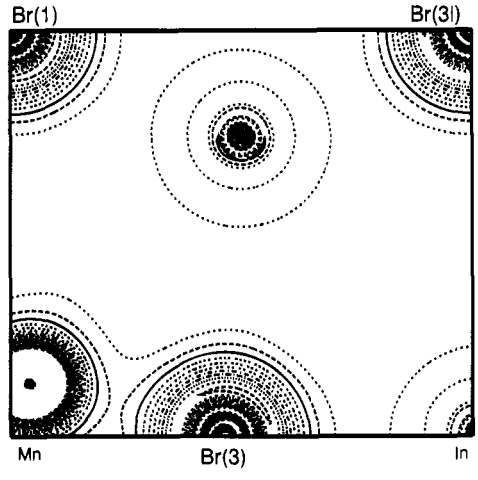

Figure 10. Same as in Figure 9 but for $InMnBr_3$.

electrons for $InMnBr_3$, in good agreement with above magnetic data and thus proving the high quality of the computational method used.

In the next step, Figures 9 and 10 show computed charge density plots for both compounds at the self-consistent level. Because of the electron density window chosen, they mainly emphasize the influence of the valence electrons. In the plots, we show those planes that contain the bromine atoms Br(1), Br(3), and Br(3l) of Figure 2, *i.e.* the three face-capping bromine atoms around the trigonal prism. There are two main observations: First, it is surprising to see that there are such large differences in the decay of the charge densities (while moving away from the nuclei) when comparing the In atom with the Fe and Br atoms. Obviously, the electron density around In is much more diffuse than around the others, very likely due to a soft crystal potential at the indium site[13] (because of *antibonding* interactions at the frontier bands) and the diffuse nature of the indium 5s orbital. In this respect, we again note that crystallographic displacement parameters of monovalent In are always significantly enlarged even with full site occupancy.

Second, and more important, there is not even a slight distortion of the indium atom's electron density visible with respect to the In−Br(3) vector, the direction into which a so-called electron "long-pair" might be expected to point. In other words, this descriptive concept is not supported by an observable quantity, *i.e.* the electron density. Thus, the distortion of the bromine coordination around indium can only be due to a geometrically optimized, significant amount of covalent In^+-Br^- bonding inside the prism (see above bonding discussion), in addition to the electrostatic interactions. A directed electron "lone-pair" hypothesis, however, is unnecessary and contradicts observation.

Acknowledgment. The author would like to thank Prof. Dr. Arndt Simon for his steady and generous support. In addition, the author gratefully acknowledges the careful X-ray data collection by Dr. Horst Borrmann, the susceptibility measurements by Eva Brücher and Dr. Reinhard K. Kremer, help in the powder and thermoanalytical investigations by Friedrich Kögel and Willi Röthenbach, as well as preparative assistance by Michael Baitinger. Expert help in the author's aberration between Ultrix and AIX operating environments was kindly provided by Armin Schuhmacher and Dr. Armin Burkhardt—the author is indebted to both of them. Also, the author would like to thank Dr. Ove Jepsen and Dr. Georges Krier for many useful suggestions upon iterating towards self-consistency. Further financial support by the Fonds der Chemischen Industrie (Frankfurt) in purchasing a portable UNIX mini-workstation is gratefully acknowledged.

Supplementary Material Available: Tables of crystallographic and structure refinement data (Tables S1 and S2) and anisotropic displacement parameters (Tables S3 and S4) (3 pages). Ordering information is given on any current masthead page.